IOP Publishing Journal of Physics B: Atomic, Molecular and Optical Physics
J. Phys. B: At. Mol. Opt. Phys. **45** (2012) 074009 (14pp) doi:10.1088/0953-4075/45/7/074009

# Optical waveform synthesizer and its application to high-harmonic generation

**Shu-Wei Huang[1], Giovanni Cirmi[1,2], Jeffrey Moses[1], Kyung-Han Hong[1], Siddharth Bhardwaj[1], Jonathan R Birge[1], Li-Jin Chen[1], Irina V Kabakova[3], Enbang Li[3], Benjamin J Eggleton[3], Giulio Cerullo[4] and Franz X Kärtner[1,2,5]**

[1] Department of Electrical Engineering and Computer Science and Research Laboratory of Electronics, Massachusetts Institute of Technology, Cambridge, MA 02139, USA
[2] Center for Free-Electron Laser Science, DESY, and Department of Physics, University of Hamburg, Notkestraße 85, D-22607 Hamburg, Germany
[3] Centre for Ultrahigh bandwidth Devices for Optical Systems (CUDOS), Institute of Photonics and Optical Science (IPOS), School of Physics, University of Sydney, NSW 2006, Australia
[4] IFN-CNR, Dipartimento di Fisica, Politecnico di Milano, Piazza L. Da Vinci 32, 20133 Milano, Italy

E-mail: kaertner@mit.edu

Received 15 September 2011, in final form 30 October 2011
Published 16 March 2012

**Abstract**
Over the last decade, the control of atomic-scale electronic motion by optical fields strong enough to mitigate the atomic Coulomb potential has broken tremendous new ground with the advent of phase-controlled high-energy few-cycle pulse sources. Further investigation and control of these physical processes, including high-harmonic generation, ask for the capability of waveform shaping on sub-cycle time scales, which requires a fully phase-controlled multiple-octave-spanning spectrum. In this paper, we present a light source that enables sub-cycle waveform shaping with a two-octave-spanning spectrum and 15 $\mu$J pulse energy based on coherent synthesis of pulses with different spectra, or wavelength multiplexing. The synthesized pulse has its shortest high-field transient lasting only 0.8 cycles (amplitude FWHM) of the centroid frequency. The benefit of the approach lies in its modular design and scalability in both bandwidth and pulse energy. Full phase control allows for the synthesis of any optical waveform supported by the amplified spectrum. A numerical study shows the uniqueness of the light source for direct isolated soft-x-ray pulse generation based on high-harmonic generation, greatly reducing and eventually even eliminating the need for gating techniques or spectral filtering. The demonstrated system is the prototype of a class of novel optical tools for attosecond control of strong-field physics experiments.

## 1. Introduction

Since the invention of mode-locked lasers, the ultrafast laser science community has seen tremendous progress towards better phase control, broader optical bandwidths, and shorter pulse durations. Better phase control and frequency comb techniques have revolutionized optical frequency metrology, optical atomic clocks and high-precision spectroscopy [1, 2]. Broader bandwidth in coherent and phase-controlled sources has also led to breakthroughs in biomedical imaging [3] and astrophysical spectrography [4]. Shorter pulse durations then have enabled ultrafast pump-probe experiments to reveal the electronic and molecular dynamics critical to the understanding of condensed matter [5], and chemical [6] and biological [7] processes. Meanwhile, the study of high-field physics such as laser plasma interaction has demanded optical pulses of ever higher pulse energies and peak powers [8]. Chirped pulse amplifiers (CPAs) have been developed and are intensively employed nowadays as the basic enabling technology for the study of high-field physics [9].

In recent years, the investigation of phenomena at the intersection of ultrafast and high-field laser physics,

---

[5] Author to whom any correspondence should be addressed.

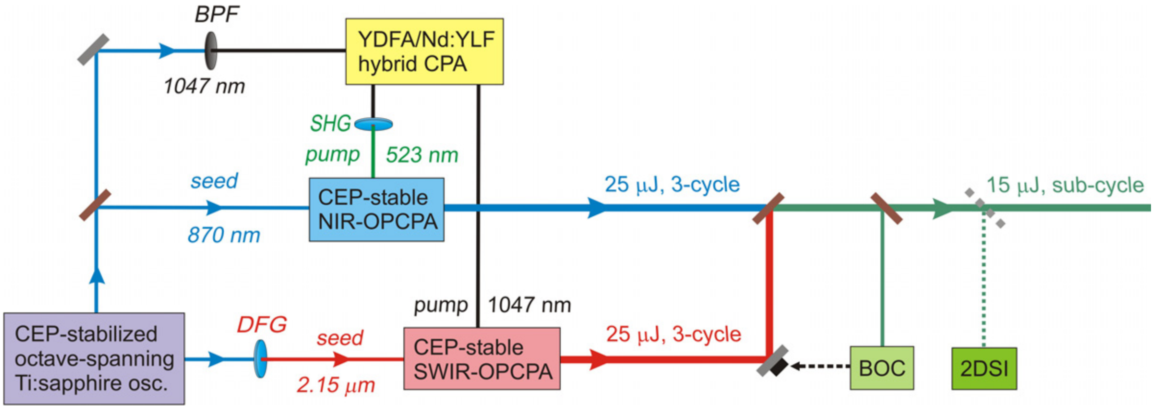

**Figure 1.** Scheme of the high-energy optical waveform synthesizer. Two CEP-stabilized, few-cycle OPCPAs centred at different wavelengths are coherently synthesized to produce isolated high-energy non-sinusoidal optical waveforms at 1 kHz repetition rate. A BOC-assisted feedback loop allows attosecond-precision relative timing stability and ensures the coherent synthesis of the two OPCPA pulses. Full control over the optical phase, enabled by the inclusion of an AOPDF in each OPCPA, allows for any optical waveform given the amplified spectrum. A 2DSI is used to characterize the synthesized pulse. BOC: balanced optical cross-correlator; 2DSI: two-dimensional spectral-shearing interferometer; YDFA: ytterbium-doped fibre amplifier; SHG: second-harmonic generation; DFG: difference-frequency generation; BPF: bandpass filter.

such as high-harmonic generation (HHG) [10] and strong-field ionization [11], has demanded that laser sources combine each of the improvements mentioned above. The development of close-to-single-cycle, carrier-envelope phase (CEP)-controlled high-energy optical pulses has already led to the generation of isolated attosecond pulses in the EUV range [12], expanding ultrafast spectroscopy to attosecond resolution [13, 14]. However, further investigation and control of these physical processes demand even more from laser technology, simultaneously requiring full phase control, multi-octave-spanning bandwidth and peak intensities of $10^{14}$ W cm$^{-2}$ and above. Such features would allow arbitrary shaping of the strong electric-field waveforms for steering ionized electron wavepackets [15] and precise control of tunnelling and multiphoton ionization events. To date, no single laser source can support a bandwidth of more than an octave [16, 17]. To extend the laser spectrum, there are in general two directions: (1) nonlinear mixing of high-intensity laser light to reach new wavelength ranges, and (2) coherent synthesis of the multi-wavelength output from intense lasers.

Supercontinuum generation [12, 18–21] and molecular modulation [22–26] are two established nonlinear mixing techniques to expand the laser bandwidth to multiple octaves. Supercontinua with a bandwidth close to two octaves and a pulse energy in the micro-joule range have been demonstrated by self-channelling of a 5 fs laser pulse in helium at high pressure, and the further dispersion management by chirped mirrors has recently led to the generation of isolated sub-optical cycle pulses [27]. On the other hand, with pulse energy at the nano-joule level, molecular modulation provides the broadest spectrum ever (more than two octaves), and periodic electric-field waveforms with square or triangle shapes have been demonstrated recently [26].

Coherent synthesis of pulses with different spectra, or wavelength multiplexing, presents another route towards obtaining a multi-octave-spanning laser spectrum. The benefit of this approach lies in its modular design and scalability in both bandwidth and pulse energy. Attempts to combine two independent mode-locked lasers have seen some success, e.g. for frequency metrology [28, 29], but are challenging because of the differential phase noise beyond the achievable feedback loop bandwidth. This problem was initially circumvented by coherently adding two pulse trains derived from the same fibre laser, resulting in the first demonstration of an isolated single-cycle optical pulse source [30]. This proved the feasibility of pulse synthesis at the nano-joule level, but achieving high pulse-energy requires synthesis of low-repetition-rate pulses, which is a challenge because of the environmental perturbations typical of high-energy amplifiers. Ultra-broadband optical parametric chirped pulse amplifier (OPCPA) is the most promising technology for producing wavelength-tunable, high-peak-power and high-average-power, few-cycle optical pulses with good pre-pulse contrast [31]. Ultra-broadband OPCPAs also maintain good CEP stability due to the low thermal load and the small dispersion required to stretch and compress the signals. Thus, the OPCPA stands out as the ideal building module for high-energy pulse synthesis. An approach to high-energy pulse synthesis based on combining the pump and its second harmonic, signal, and idler of a multi-cycle optical parametric amplifier is being investigated and periodic non-sinusoidal electric-field waveforms under a multi-cycle envelope have been demonstrated recently [32].

In this work, we demonstrate the coherent synthesis of the already few-cycle pulses from two ultra-broadband OPCPAs, working in the near-infrared (NIR) and the short-wavelength infrared (SWIR) respectively. Our source allows the generation of isolated high-energy non-sinusoidal optical waveforms with full phase control capability over the spectra spanning close to two octaves [33]. Figure 1 shows a schematic of the system. It starts with an actively CEP-stabilized octave-spanning Ti:sapphire oscillator. The output of the oscillator is used to seed the two OPCPAs as well as the ytterbium-doped fibre amplifier (YDFA)/Nd:YLF hybrid

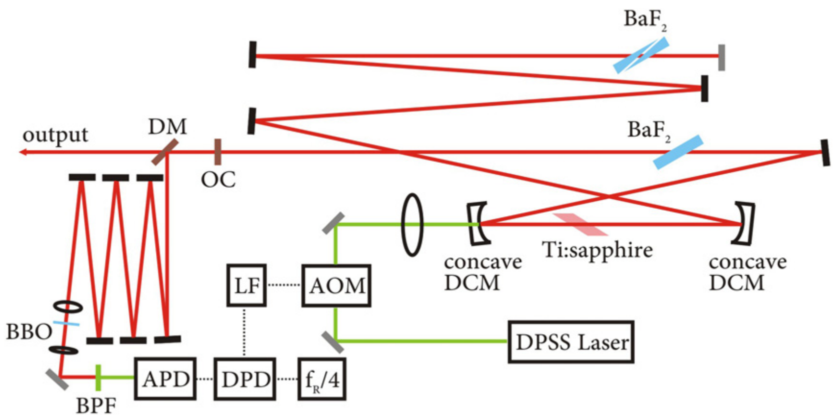

**Figure 2.** Scheme of the CEP-stabilized octave-spanning Ti:sapphire oscillator. The output of the oscillator is used to seed the two OPCPAs as well as the YDFA/Nd:YLF hybrid CPA, which pumps the two OPCPAs. DM: dichroic mirror; OC: output coupler; DCM: double-chirped mirror; DPSS laser: diode-pumped solid-state laser; BPF: bandpass filter; APD: avalanche photodiode; DPD: digital phase detector; LF: loop filter; AOM: acousto-optic modulator. All DCMs are coloured in black and all silver mirrors are coloured in grey.

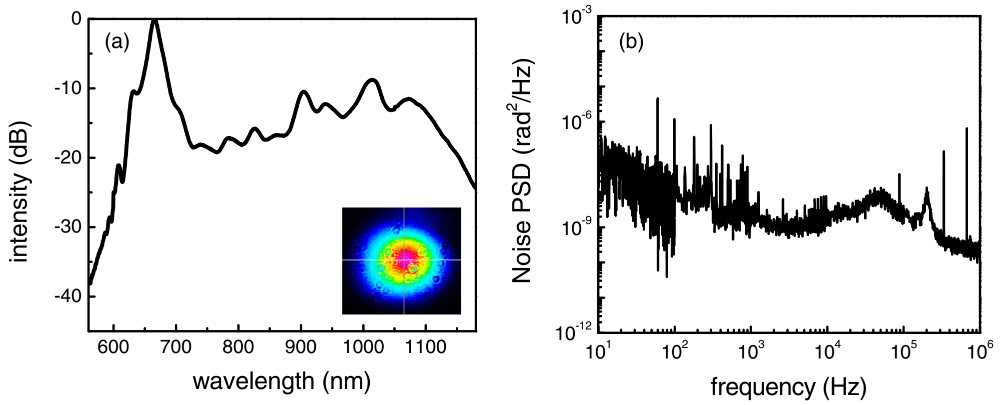

**Figure 3.** (a) The output spectrum of the oscillator. An octave is reached at the spectral density of −25 dB. The lower inset is the output beam profile. (b) The PSD of the oscillator's residual CEP fluctuation. The integrated phase noise is 60 mrad.

CPA, which pumps the two OPCPAs. Outputs from the two OPCPAs are combined in a broadband neutral beamsplitter. A feedback loop based on a balanced optical cross-correlator (BOC) [34], allowing attosecond-precision relative timing stability, is implemented to ensure the coherent synthesis of the two pulses. Furthermore, the inclusion of an acousto-optic programmable dispersive filter (AOPDF) in each OPCPA allows independent spectral phase and amplitude adjustment of each pulse, enabling control and optimization of the synthesized waveform. Overall, a pulse energy of 15 $\mu$J is obtained with a bandwidth close to two octaves and the shortest high-field transient lasting only 0.8 cycles (amplitude FWHM) of the centroid frequency. By simulation, we present an example of the unique features of our source as a driver for HHG.

The paper is organized as follows. Section 2 shows the setup and characterization of the Ti:sapphire oscillator which is used as the very first component for driving the whole laser architecture. Section 3 presents the mechanisms for generating the seeds and the pumps of both OPCPAs. Section 4 shows the setup and characterization of the OPCPAs. Section 5 presents the mechanisms for synthesizing the two pulses and the control over the important parameters. An example illustrating the unique features of our source as a driver for HHG is presented in section 6. Finally, we summarize our results in section 7.

## 2. Ti:sapphire oscillator

Figure 2 is the schematic of the Ti:sapphire oscillator (IdestaQE Octavius-85M) and it is similar to the one described in [16]. Pumped with 6 W of 532 nm light (Coherent Verdi V6), the oscillator outputs an average power of 200 mW with a repetition rate of 85 MHz. The optical cavity is set up in an astigmatism-compensated x-folded geometry employing two concave double-chirped mirrors (DCMs) with 75 mm radius of curvature. The dispersion of the Ti:sapphire gain crystal and the air within the cavity is precisely compensated by DCM pairs, a BaF$_2$ plate and a BaF$_2$ wedge pair. BaF$_2$'s low ratio of the group-delay dispersion and the third-order dispersion allows the design of octave-spanning DCMs with 99.9% reflectivity from 580 to 1200 nm. Finally, a broadband quarter-wave ZnSe/MgF$_2$ output coupler that transmits more on the spectral edges than the centre helps reshape the output spectrum to achieve a bandwidth of an octave. Figure 3(a) shows the output spectrum of the oscillator, showing that the octave is reached at the spectral density of −25 dB.

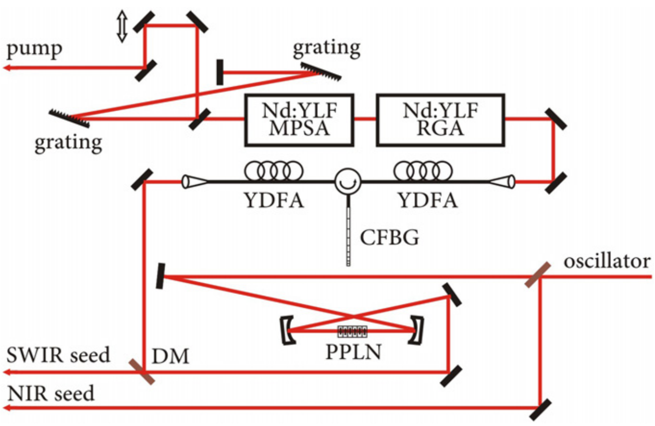

**Figure 4.** Generation of the seed pulses for the OPCPAs and all-optical synchronization. 10% of the oscillator output is used to seed the NIR-OPCPA channel while the rest of the output is focused into a 2 mm MgO-doped PPLN crystal, wherein intrapulse DFG creates 2.15 $\mu$m seed pulses for the SWIR-OPCPA channel. After the intrapulse DFG stage, a DM is used to pick up the 1047 nm component for seeding the YDFA/Nd:YLF hybrid CPA, which pumps the two OPCPAs. The CFBG has a chirp rate of 440 ps nm$^{-1}$, enough to avoid B-integral-related damage in the Nd:YLF RGA and the two MPSAs.

The output of the oscillator is split in a dichroic mirror (DM) that transmits the light from 650 to 1050 nm and reflects the light below 650 nm and above 1050 nm. The transmission port is used for seeding the rest of the system, and the reflection port is directed into a $f$–$2f$ self-referencing interferometer for locking the CEP of the oscillator. A collinear configuration is chosen for its robustness against environmental noise. Six bounces on DCMs are employed for proper group-delay adjustment to maximize the CEP-beat signal. After the DCM-based delay line, the beam is focused onto a 1 mm thick type-I $\beta$-barium borate (BBO) crystal for second-harmonic generation (SHG). The emitted SHG light and the fundamental light are spatially filtered using an iris diaphragm, spectrally filtered using a 10 nm interference bandpass filter (BPF) centred at 570 nm, and directed to a fast avalanche photodiode (MenloSystems APD210). The CEP-offset frequency is locked to a fourth of the oscillator's repetition rate through a phase-locked loop that feeds back to an acousto-optic modulator regulating the pump power, thus shifting the CEP-offset frequency. A digital phase detector is used to increase the capture range ($\pm 32\pi$) beyond a traditional analogue mixer ($\pm\pi/2$). Figure 3(b) shows the power spectral density (PSD) of the residual CEP fluctuations and the integrated CEP rms phase error (10 Hz to 1 MHz) is 60 mrad. Since the major source of CEP is the intracavity intensity fluctuations introduced by pump laser noise, the phase noise rapidly decays beyond the relaxation frequency that is typically a few hundred kHz. Therefore, the upper limit of the measurement is set to be 1 MHz to exclude the high-frequency noise contributed by the electronics noise floor rather than the laser phase noise itself.

## 3. Seed and pump

Figure 4 shows the all-optical synchronized seed and pump generation scheme. A broadband 10/90 beamsplitter divides the oscillator output into two parts: 10% of the oscillator output is directed to the NIR-OPCPA channel centred around 870 nm while the rest of the output is focused into a 2 mm MgO-doped periodically poled congruent lithium niobate (MgO:PPcLN) crystal with a poling period of 13.1 $\mu$m, wherein intrapulse difference-frequency generation (DFG) creates 2.15 $\mu$m seed pulses for the SWIR-OPCPA channel. Figures 5(a) and (b) are the spectrum of the two seeds, both reaching a bandwidth of more than half an octave (full width at −20 dB).

After the intrapulse DFG stage, a DM and a 4 nm BPF is used to pick up the 1047 nm component for seeding the YDFA/Nd:YLF hybrid CPA, which pumps the two OPCPAs. To suppress amplified spontaneous emission in the Nd:YLF regenerative amplifier (RGA), the seed is pre-amplified to 3 pJ in two YDFAs. The gain of the YDFAs is kept to 10 to avoid parasitic lasing at 1030 nm. The Nd:YLF CPA system consists sequentially of a chirped fibre Bragg grating (CFBG) stretcher, an Nd:YLF RGA followed by two Nd:YLF multi-pass slab amplifiers (MPSAs), and a diffraction grating compressor. The CFBG has a length of 10 cm, super-Gaussian apodization and a chirp rate of 440 ps nm$^{-1}$. The grating was inscribed

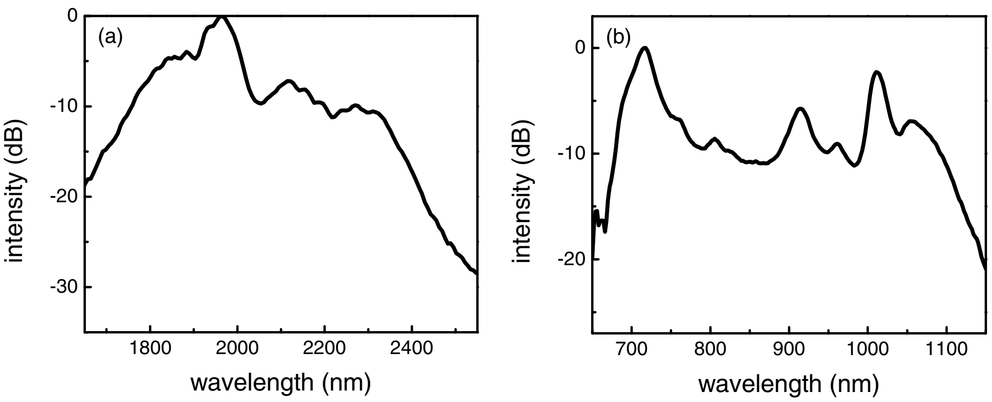

**Figure 5.** (a) The seed spectrum of the SWIR-OPCPA. (b) The seed spectrum of the NIR-OPCPA. Both seeds reach a bandwidth of more than half an octave and cover the phase-matching bandwidth of the corresponding OPCPAs.

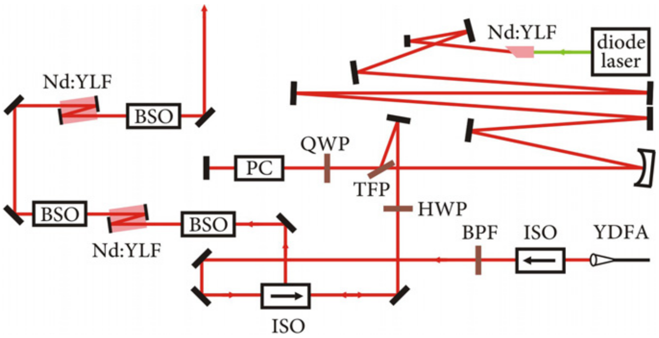

**Figure 6.** Scheme of the Nd:YLF hybrid CPA, including a RGA and two Nd:YLF MPSAs. The RGA output energy is 1.05 mJ with a shot-to-shot rms energy fluctuation better than 0.5% and the output bandwidth is 0.25 nm. The RGA output pulse is then further amplified in the two three-pass Nd:YLF MPSAs. Overall, the two Nd:YLF MPSAs offer a gain of 6.3 and an output pulse energy of 5.7 mJ is obtained. YDFA: ytterbium-doped fibre amplifier; ISO: optical isolator; BPF: bandpass filter; HWP: half waveplate; TFP: thin film polarizer; QWP: quarter waveplate; PC: Pockels cell; BSO: beam shaping optics.

in Nufern PS1060 photosensitive fibre using a phase-mask scanning technique in a Sagnac interferometric configuration. The pulse duration after the Nd:YLF RGA is 110 ps with a bandwidth of 0.25 nm, enough to avoid B-integral-related damage in the Nd:YLF MPSAs.

Figure 6 shows the schematics of the Nd:YLF RGA (High-Q Laser) and the Nd:YLF MPSAs (Q-Peak). All Nd:YLF crystals are oriented to operate at the 1047 nm emission line, utilizing the high gain quality. In the RGA, the Nd:YLF crystal is back-coated such that the 1047 nm light is reflected while the 798 nm diode pump is transmitted. A quarter waveplate, a Pockels cell operating at 0° and $\lambda/4$, and a thin-film polarizer control the injection and ejection of the RGA pulses. The total cavity length is 1.5 m. To reduce the loss associated with the thermal lensing, a quasi-CW pumping scheme is employed: the crystal is pumped for 450 $\mu$s until the seed is injected. A single-pass small-signal gain of 2 can be achieved and the RGA output energy is 1.05 mJ with a shot-to-shot rms energy fluctuation better than 0.5%. The overall RGA gain is more than 90 dB and the output bandwidth is reduced to 0.25 nm due to the strong gain narrowing. The RGA output pulse is then further amplified in the two three-pass Nd:YLF MPSAs. Each Nd:YLF crystal is 28 mm long, 2 mm by 6 mm in aperture, and side pumped with 78 W optical power. Due to the side pumping geometry, the asymmetric thermal lensing introduces astigmatism to the output pulse. A telescope with tilted lenses and cylindrical lenses is thus implemented after each MPSA to correct the astigmatism. Overall, the two Nd:YLF MPSAs offer a gain of 6.3 and an output pulse energy of 5.7 mJ is obtained. The pulse is then compressed using a gold-coated grating pair, where the gratings have a groove density of 1800 lines mm$^{-1}$ and a diffraction efficiency of 90%. The separation between the two gratings is set to 2.7 m with multiple bounces off dielectric mirrors to achieve a compact setup. The throughput of the diffraction grating compressor is ~65% and a compressed pulse duration of 12 ps (~1.3× of the transform limit) is measured using a single-shot autocorrelator. A half waveplate and a polarization beamsplitter then divide the pulse into two parts where 1 mJ is used to pump the SWIR-OPCPA and 2 mJ is first frequency doubled in a 1 cm lithium triborate crystal before being used to pump the NIR-OPCPA. The frequency doubling process has a conversion efficiency of ~45% and further push to higher conversion is undesirable due to the loss of beam quality.

For the stable operation of OPCPAs, pump and signal pulses must be synchronized to within less than a fraction of their durations. Employment of picosecond pumps, which are advantageous over nanosecond pumps in terms of gain-bandwidth product [35], thus precludes the use of electronic synchronization methods. Thanks to the octave-spanning spectrum of the Ti:sapphire oscillator, direct seeding of a YDFA/Nd:YLF hybrid CPA is possible and thus the pump and signal are optically synchronized. A study of the optical synchronization scheme [36] shows that the residual timing jitter and drift over an hour are well below 1 ps, less than 10% of our pump duration. Day-to-day timing shift between the pump and signal pulses has been observed, but the amount of shift can be easily accommodated by tuning the optical delay line of the pump.

## 4. Optical parametric chirped pulse amplifiers

Figure 7 shows the modular schematics of both OPCPAs. The signal is first stretched by stretcher-1 to 40–50% of the pump pulse duration and then pre-amplified in the first OPCPA stage to 1–2 $\mu$J with a gain of 50–60 dB. The pre-amplified pulse is further stretched to 70–80% of the pump pulse duration by stretcher-2 and finally the signal is amplified to 20–30 $\mu$J with a gain of 20–30 dB. Of note, the gain of the pre-amplifier and the power-amplifier are significantly different and thus the stretching ratios for the signal have to be different for simultaneously optimizing energy conversion, amplification bandwidth and signal-to-noise ratio [37]. Between the two OPCPA stages, a fine phase management setup (for example, the AOPDF in our system) and a spatial filter for mode cleaning and superfluorescence suppression are included. While the fine phase management

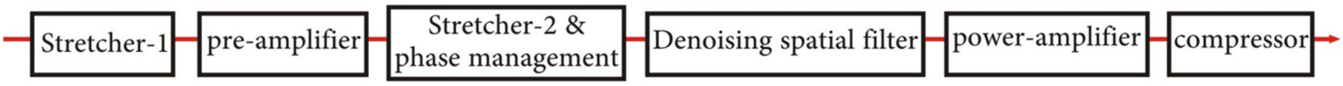

**Figure 7.** Modular scheme of the two-stage OPCPA. The signal is first stretched by stretcher-1 and then pre-amplified in the first OPCPA stage. The pre-amplified pulse is further stretched by stretcher-2 and finally amplified in the second OPCPA stage. Between the two OPCPA stages, a phase management setup and a spatial filter for mode cleaning and superfluorescence suppression are included. At the end, a bulk material is used to compress the pulses.

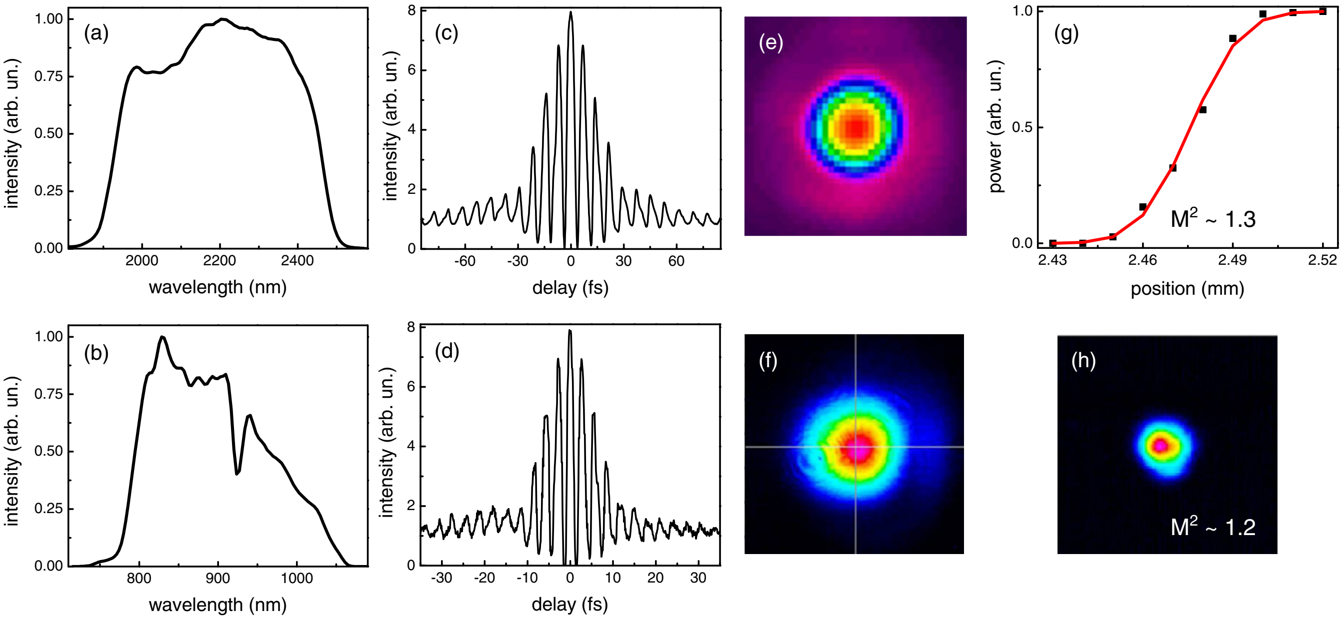

**Figure 8.** Characteristics of the OPCPAs. (a) The output spectrum of the SWIR-OPCPA. (b) The output spectrum of the NIR-OPCPA. (c) The interferometric autocorrelation trace of the SWIR-OPCPA pulses. (d) The interferometric autocorrelation trace of the NIR-OPCPA pulses. (e) The far-field beam profile of the SWIR-OPCPA. (f) The far-field beam profile of the NIR-OPCPA. (g) The knife-edge measurement of the near-field beam profile of the SWIR-OPCPA, indicating an $M^2$ value of 1.3. (h) The near-field beam profile of the NIR-OPCPA, indicating an $M^2$ value of 1.2.

setup enables control and optimization of the synthesized waveform, it inevitably introduces signal loss and thus it is generally better to place it between the pre-amplifier and the power-amplifier for simultaneous optimization of output power and superfluorescence suppression: if placed before the pre-amplifier, its losses directly reduce the signal-to-noise ratio, which is set by the ratio of seed power to equivalent noise energy in vacuum modes [38]. Placed after the power-amplifier, its losses reduce the output power. An effective spatial filter, created by setting the pump beam width less than a half of the signal beam width and placing the nonlinear crystal a few diffraction lengths away from the signal focus, improves the beam quality and eliminates the phase-matched, superfluorescence-dominated high-order spatial modes of the signal. If the initial signal-to-noise ratio is particularly low, such as for our SWIR-OPCPA, an additional iris diaphragm is implemented for the same purpose. At the end, a bulk material is used to compress the pulses to their transform limit.

For the SWIR-OPCPA [39], a 30 mm bulk silicon block is used as stretcher-1 to stretch the signal to 5 ps. The signal is pre-amplified to 1.5 $\mu$J in a 3 mm MgO:PPcLN with a poling period of 31.0 $\mu$m, pumped with 150 $\mu$J pulses. The pre-amplified pulse is further stretched to 9.5 ps by an AOPDF which also serves as a fine phase management setup. Of note, the AOPDF can also shape the output spectrum but care has to be taken to ensure sufficient seed energy for the power-amplifier. The gain medium for the power-amplifier is a 3 mm MgO-doped periodically poled stoichiometric lithium tantalate crystal (MgO:PPsLT) with a poling period of 31.4 $\mu$m, pumped with 750 $\mu$J pulses. The output pulses have 25 $\mu$J energy and can be compressed to nearly transform-limited 24 fs duration in a 300 mm broadband anti-reflection coated Suprasil-300 glass block. For the NIR-OPCPA [33], a Brewster prism pair with 1 m apex-to-apex distance stretches the signal to 5 ps. The signal is pre-amplified to 2 $\mu$J in a double-pass, non-collinear (2.4° pump-signal angle) geometry in a type-I, 5 mm long BBO crystal cut at $\theta = 24°$, and pumped with 250 $\mu$J pulses. The pre-amplified pulse is further stretched to 6.2 ps by a combination of a Treacy grating pair and an AOPDF. The gratings have a groove density of 300 lines mm$^{-1}$ and the separation between the two gratings is 82 mm. The Treacy grating pair is included in order to balance the excess high-order dispersion introduced by the Brewster prism pair. Additionally, the CEP drift caused by a Treacy grating pair due to temperature fluctuation is opposite in sign to that of a Brewster prism pair [40] and thus the inclusion of a Treacy grating pair improves the long-term CEP stability. Again the AOPDF also serves as a fine phase management setup here. The gain medium for the power-amplifier is the same as the first OPCPA stage, but pumped with 650 $\mu$J pulses. The output pulses with an energy of 25 $\mu$J are then compressed to 9 fs in a 40 mm Brewster-cut N-LaSF9 glass block.

Figures 8 and 9 show the characterization of the two OPCPAs. Both OPCPAs reach bandwidths of more than half an octave (full width at −20 dB) and the combined spectrum spans over 1.8 octaves. The OPCPA outputs can be both compressed to within 10% of their transform-limited pulse durations, measured with interferometric autocorrelators (figures 8(c) and (d)). Figures 8(e) to (h) show the near-field and far-field beam profiles, showing clean fundamental Gaussian modes with good $M^2$ values. As the CEP-offset frequency of the Ti:sapphire oscillator is locked to one fourth

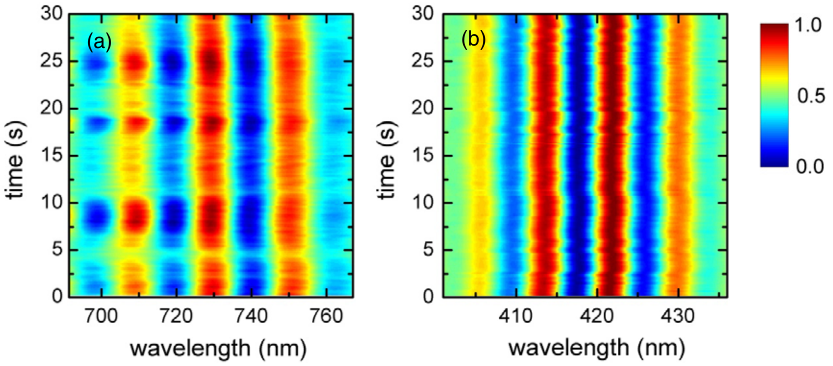

**Figure 9.** CEP stability measurements of the OPCPAs. (a) $f$–$3f$ interferogram of the SWIR-OPCPA with five-shot integration over 30 s, measuring an rms CEP fluctuation of 127 mrad. (b) $f$–$2f$ interferogram of the NIR-OPCPA with five-shot integration over 30 s, measuring an rms CEP fluctuation of 135 mrad.

of its own repetition rate and the same frequency is used as the master clock of the whole system, the CEP of the NIR-OPCPA is actively stabilized. On the other hand, the CEP of the SWIR-OPCPA is in addition passively stabilized due to the intrapulse DFG process used to produce the seed [41]. Using an $f$–$3f$ interferometer and five-shot integration, the CEP stability of the SWIR-OPCPA was verified with an rms fluctuation of 127 mrad (figure 9(a)). An $f$–$2f$ interferometer with five-shot integration was used to verify the CEP stability of the NIR-OPCPA, which shows an rms fluctuation of 135 mrad (figure 9(b)). CEP stabilization of both OPCPAs is an important first step toward the coherent synthesis. Its role and the effect of the residual fluctuations will be discussed in the following sections.

## 5. Coherent synthesis

Outputs from the two OPCPAs are individually collimated with the diameter of the SWIR-OPCPA 2.5 times larger than that of the NIR-OPCPA and then combined in a broadband neutral beamsplitter. When focused, the two beams at the focus have the same spot size and this ‘constant waist width’ configuration [42] offers the unique property that the temporal pulse form remains unchanged upon propagation, whereas distortion appears in the near-field when the ‘constant diffraction length’ configuration is used [42]. The overall spectrum spans over 1.8 octaves and the energy of the synthesized pulse is 15 $\mu$J.

The phase coherence between the two OPCPA pulses is ensured by the following procedure (figure 10): we first ensure stabilization of the CEPs of the NIR-OPCPA pulses ($\phi_1$) and SWIR-OPCPA pulses ($\phi_2$) (see figure 9), and then stabilize the relative timing between the two OPCPA pulses ($\Delta t$). Precise stabilization of these three parameters is required for coherent synthesis of the two OPCPA pulses, and subsequent control of each parameter allows precise waveform shaping.

As described in the previous section, the CEP of the SWIR-OPCPA is passively stabilized up to residual rms fluctuations of 127 mrad while the CEP of the NIR-OPCPA is actively stabilized to within an rms fluctuation of 135 mrad. To stabilize the relative timing, a feedback loop based on a BOC is implemented [34]. A BOC is the optical equivalent of a balanced microwave phase detector and is particularly suitable for measuring slow timing drifts with attosecond precision because the balanced detection configuration cancels the amplitude noise. Figure 11(a) shows the schematics of the BOC. One part of the combined beam is directed to the BOC which consists of two nearly identical cross-correlators using 200 $\mu$m thick BBO crystals, phase matched for sum-frequency generation of 870 nm light and 2.15 $\mu$m light. Use of the SWIR-OPCPA delay stage and a 4 mm thick calcium fluoride ($CaF_2$) window between cross-correlators sets the group delay between pulses to +25 fs in one cross-correlator and −25 fs in the other. An additional ∼2 mm thick calcium fluoride window ensures zero group delay ($\Delta t = 0.0$ fs) between both

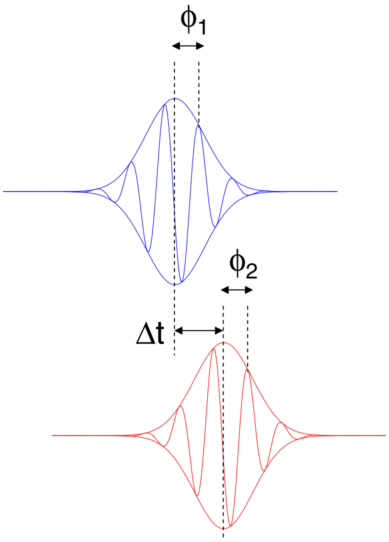

**Figure 10.** Illustration showing a way to establish the phase coherence between the two OPCPA pulses. The CEPs of the NIR-OPCPA pulses ($\phi_1$) and the SWIR-OPCPA pulses ($\phi_2$) are first stabilized independently and then the relative timing between the two OPCPA pulses ($\Delta t$) is stabilized. Precise stabilization of these three parameters is required for coherent synthesis of the two OPCPA pulses, and subsequent control of each parameter allows precise waveform shaping.

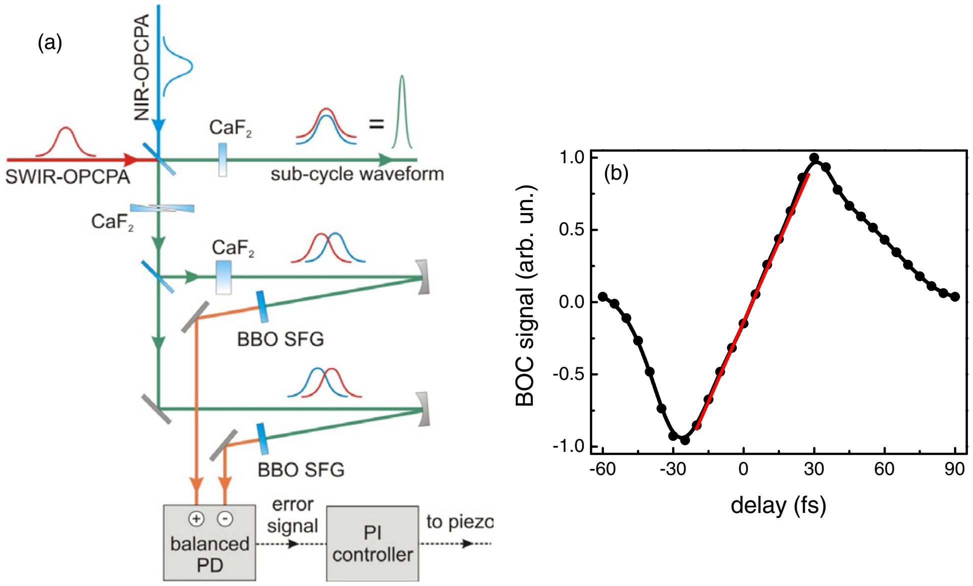

**Figure 11.** (a) Scheme of the BOC-assisted feedback loop for the stabilization of the relative timing. (b) BOC signal as a function of the relative timing between the two OPCPA pulses. The red line indicates the linear operation regime. BOC: balanced optical cross-correlator; SFG: sum-frequency generation; PD: photodetector.

pulses at the combined output. For deviations from this zero-delay configuration of up to ±20 fs, the photodetector signal is linearly proportional to the time difference and thus can be used as the error signal fed to the loop filter in the feedback system (figure 11(b)). Furthermore, in the vicinity of the zero crossing, the setup delivers a balanced signal and thus the amplitude noise of each OPCPA output does not affect the detected error signal. Since the balanced operation is key to attosecond precision, it is thus not desirable to offset the locking point as the mechanism to change the relative timing ($\Delta t$). Instead, the wedge pair in the path to the BOC should be used to change the relative timing ($\Delta t$) without offsetting the locking point and introducing additional dispersion to the combined output.

Since the OPCPAs and pump laser system are all seeded by a single octave-spanning Ti:sapphire oscillator, the two OPCPA pulses are already synchronized to within environmental fluctuations. Freely running, the system displays a peak-to-peak relative timing drift of 30 fs over a measurement time of 10 s, with the main noise contribution below 30 Hz (figure 12). Feedback control of the SWIR-OPCPA's path length over a bandwidth of 30 Hz reduces the relative timing drift to 250 as, less than 5% of the oscillation period of the SWIR-OPCPA (7.2 fs).

Since these three parameters (the CEP of the NIR-OPCPA, $\phi_1$, the CEP of the SWIR-OPCPA, $\phi_2$, and the relative timing between the two OPCPAs, $\Delta t$) significantly influence the synthesized electric-field waveform, it is important to make sure that the residual jitter is sufficiently small to impart only a negligible effect. Figure 13 shows the synthesized electric-field waveform with the rms value of each residual jitter added to the respective parameters (black dotted line) superimposed with the unperturbed waveform (green solid line). To quantify the waveform difference, we calculate the relative squared error (RSE) in a 10 fs time window that covers the main pulse as well as the two satellite pulses. Currently the 250 as relative timing jitter results in the largest waveform change (2.22% RSE), but it can be further reduced using a broader feedback bandwidth.

A two-dimensional spectral-shearing interferometer (2DSI) [43], a variation of spectral-shearing interferometry [44], is used to characterize the synthesized pulse. In 2DSI, there is no delay between the two spectrally shifted copies of the measured pulse and thus no spectral interference is present. Rather, the group delay at each wavelength is encoded in the phase of the interference fringes along a wavelength-independent axis, created by scanning the relative phase between the two spectrally shifted copies ($\phi_{gd}$). Thus, 2DSI is free from the challenge of calibrating interferometer delay. The two-dimensional intensity plot can be expressed as

$$\begin{aligned} I(\omega,\phi_{gd}) &= 2|A(\omega)A(\omega-\Omega)|\cos\{\phi_{gd}+[\phi(\omega)+\phi_{CE}] \\ &\quad -[\phi(\omega-\Omega)+\phi_{CE}]\}+D.C. \\ &\approx 2|A(\omega)A(\omega-\Omega)|\cos[\phi_{gd}+\tau_{gd}(\omega-\Omega/2)\cdot\Omega]+D.C., \end{aligned} \tag{1}$$

where $\phi(\omega)$ is the spectral phase, $\Omega$ is the shear frequency, $\phi_{CE}$ is the CEP and $\tau_{gd}(\omega)$ is the wavelength-dependent group delay. As shown in equation (1), the spectral phases and the relative timing of the two OPCPA pulses can be determined, but not the CEPs as a constant phase is cancelled in the interference of the two spectrally shifted copies. However, the CEPs can be measured *in situ* when strong-field experiments are conducted. For example, it has been shown that the actual CEP value can be determined by monitoring of the asymmetry between above-threshold ionization spectra obtained at opposite directions with respect to the laser polarization [45]. In this way, the CEPs ($\phi_1$ and $\phi_2$) not only can be changed by tuning of any dispersive elements such as

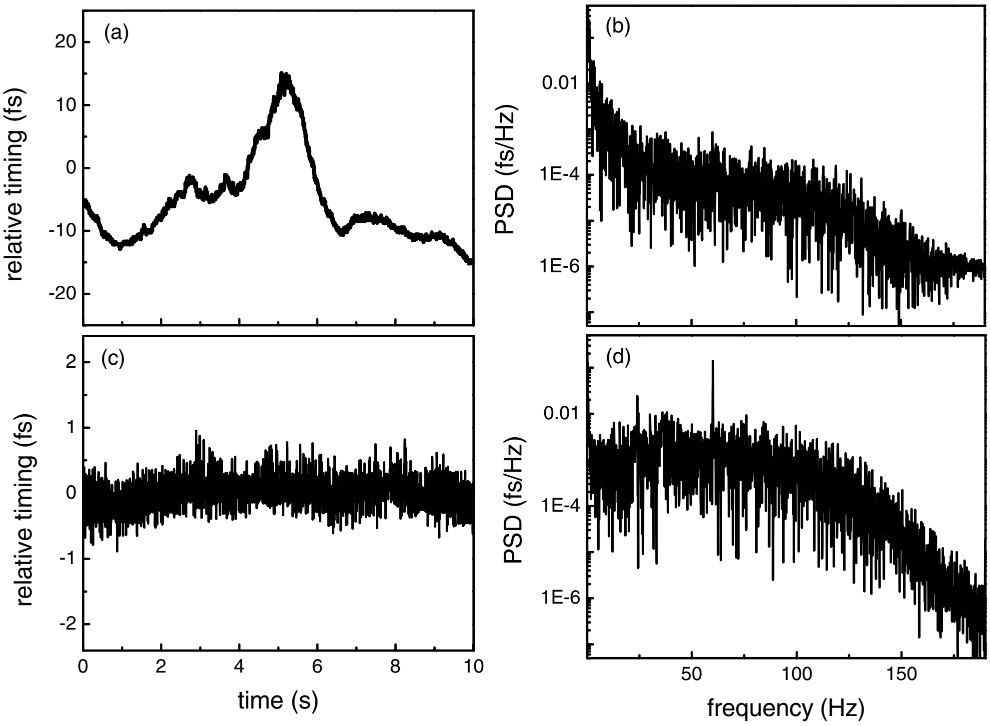

**Figure 12.** Characteristics of the relative timing between the two OPCPA pulses. (a) Without the feedback loop, the relative timing experiences a drift of 30 fs over 10 s. (b) The PSD of the relative timing fluctuation, showing the main noise contribution, is below 30 Hz. (c) With the feedback loop, the rms relative timing jitter is reduced to 250 as over 10 s. (d) The PSD of the residual relative timing jitter. PSD: power spectral density.

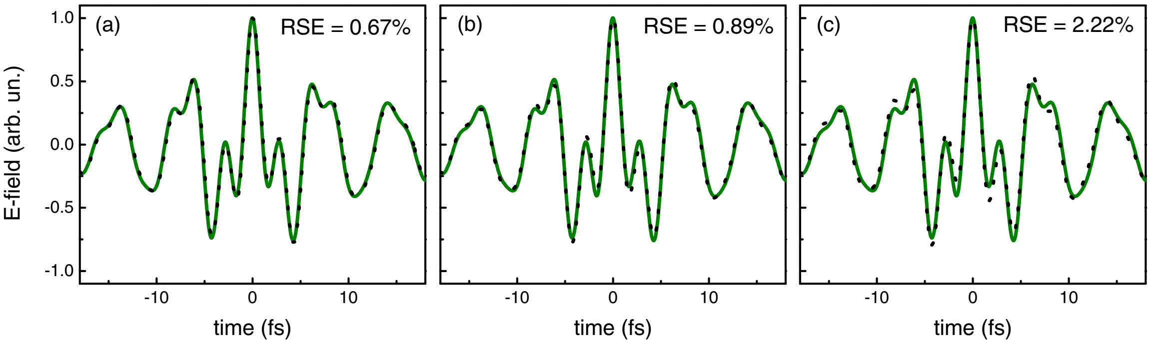

**Figure 13.** Waveforms under rms residual jitters. While the green solid lines are the unperturbed waveform, the black dotted lines are obtained by adding 135 mrad to $\phi_1$ in (a), adding 127 mrad to $\phi_2$ in (b), and adding 250 as to $\Delta t$ in (c). RSE: relative squared error.

the AOPDFs, they can also be determined without ambiguity and with high precision.

Figure 14 shows the schematics of the 2DSI. The synthesized pulse is first split by a beam sampler whose second surface is anti-reflection coated. A part of the beam (4%) is Fresnel reflected and only guided via silver mirrors before being mixed in a 40 $\mu$m type-II BBO. The other part of the beam (96%) passes through the beam sampler and is highly stretched before being split again by a cube beamsplitter, routed to the BBO and mixed with the unchirped pulse. The portion mixed with the unchirped pulse is purely derived from the NIR-OPCPA to ensure that there is a definite reference for the measured wavelength-dependent group delay throughout the whole spectrum from 700 to 2500 nm. Two collinear, temporally overlapped, but spectrally sheared upconverted pulses are then generated from the mixing of the unchirped pulse and the two chirped pulses. The shear frequency is set at 14.5 THz such that a temporal window over which the pulse can be reliably measured without phase ambiguity is 70 fs. To observe the interference between the two upconverted pulses, which encodes the wavelength-dependent group-delay information, the delay of one of the highly chirped pulses is scanned over a few optical cycles. Due to the strong chirp, the scanning of the delay over a few optical cycles can be approximated as a pure phase modulation ($\phi_{gd}$). The spectrum of the upconverted signal is recorded as a function of this delay, yielding a two-dimensional intensity plot that is shown in figure 15(a). The interpretation of the 2DSI data is relatively

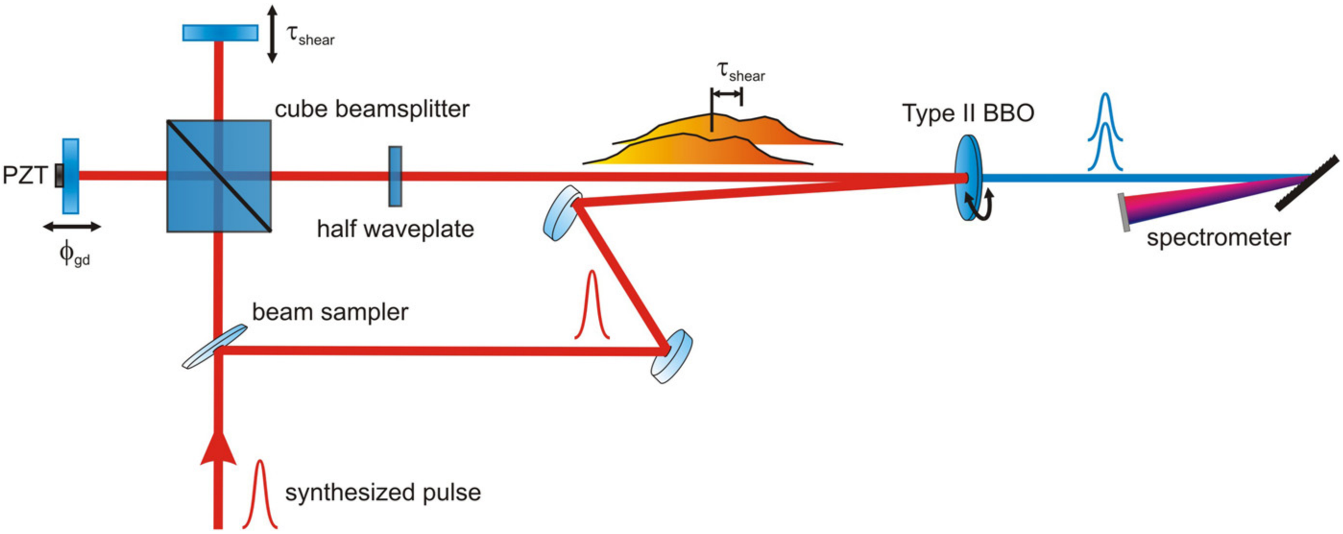

**Figure 14.** Scheme of the 2DSI for characterizing the synthesized pulse. To observe the interference between the two spectrally shifted upconverted pulses, which encodes the wavelength-dependent group-delay information, the delay of one of the highly chirped pulses is scanned by a PZT-mounted mirror over a few optical cycles. Due to the strong chirp, the scanning of the delay can be approximated as a pure phase modulation ($\phi_{\mathrm{gd}}$).

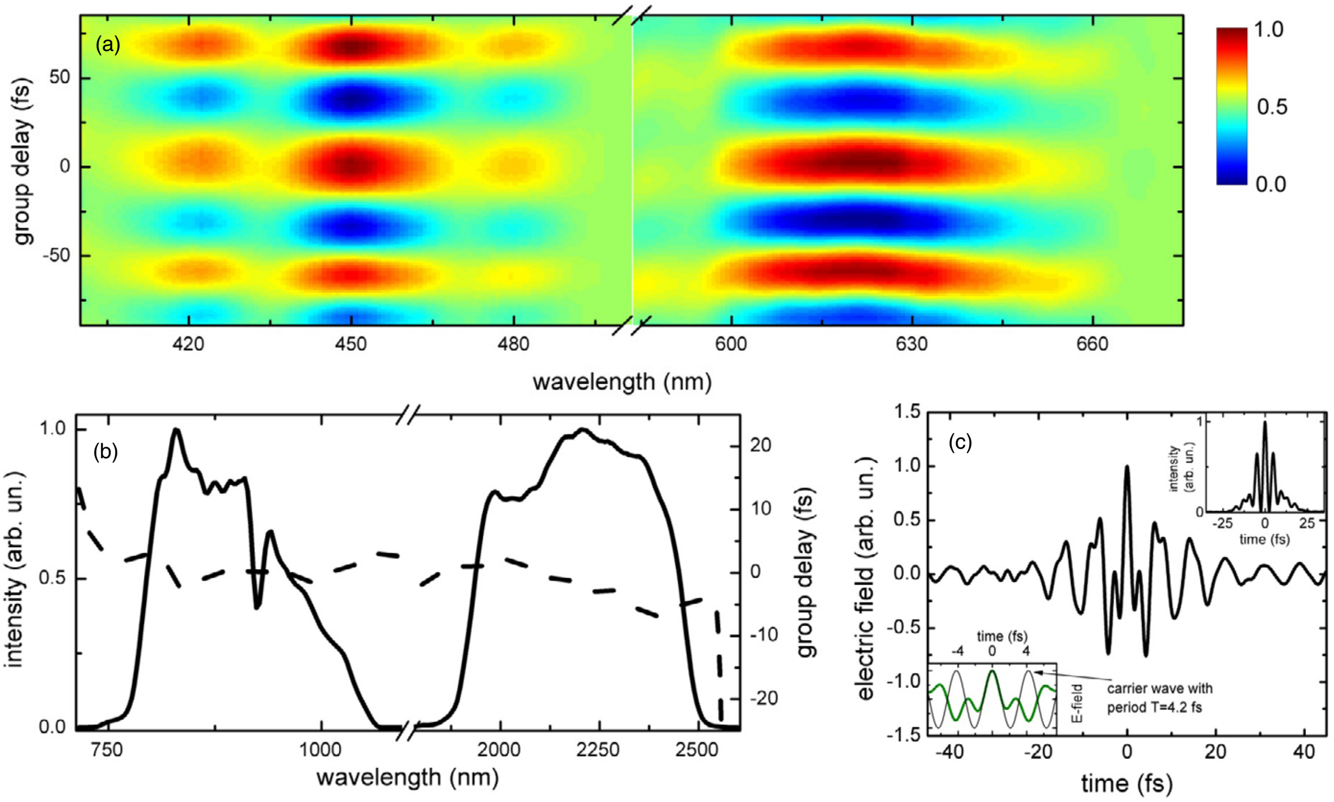

**Figure 15.** Characteristics of the synthesized pulse. (a) 2DSI data of the synthesized pulse. (b) The extracted wavelength-dependent group delays superimposed on the OPCPA output spectra. (c) The synthesized electric-field waveform assuming CEPs ($\phi_1 = 650$ mrad, $\phi_2 = -750$ mrad) optimal for achieving the shortest high-field transient, which lasts only 0.8 cycles (amplitude FWHM) of the centroid frequency. Lower inset: the synthesized waveform is superimposed with the electric field oscillating at the centroid frequency, showing that the synthesized waveform is non-sinusoidal and the main feature lasts less than an optical cycle. Upper inset: corresponding intensity profile.

straightforward: each spectral component is vertically shifted in proportion to its group delay.

Figure 15(b) plots (dashed lines) the wavelength-dependent group delay of the synthesized pulse extracted from the 2DSI measurement (figure 15(a)). It shows that the two OPCPA pulses are temporally overlapped and each is well compressed to within 10% of its transform-limited pulse duration. Figure 15(c) plots a synthesized electric-field waveform and intensity profile assuming the CEPs ($\phi_1 = 650$ mrad, $\phi_2 = -750$ mrad) optimal for achieving the shortest high-field transient, which lasts only 0.8 cycles (amplitude FWHM) of the centroid frequency ($\lambda_c = 1.26\ \mu$m). The lower inset of figure 15(c) clearly shows that the synthesized electric-field waveform is non-sinusoidal and the main feature lasts less than an optical cycle. Due to the large gap in the combined spectrum, there are wings 4.8 fs from the central peak as shown in figure 15(c). As we will show in the following section, for processes initiated by strong-field ionization, these wings have a negligible effect. For more demanding applications, the wings can be suppressed by extension of the coherent wavelength multiplexing scheme to include a third OPCPA, centred at 1.5 $\mu$m [46], to fill the spectral gap.

## 6. Attosecond pulse generation

The synthesized waveforms are important for optimizing the HHG process, which is to date the only demonstrated technique for generating isolated attosecond pulses. Due to the inherent half-cycle symmetry of the HHG process, novel techniques such as polarization gating [47, 48], two-colour gating [49, 50], ionization gating [51], double optical gating [52] and ground-state depletion gating [53] are required to produce isolated attosecond pulses when the driving pulse duration is more than an optical cycle. These techniques open up the field of attosecond science, but the efficiency is fundamentally limited because energy outside the gating period is not used. Single-cycle and sub-cycle driving pulses can be used for generating the shortest and most intense isolated attosecond pulses with a given driving pulse energy. Moreover, by shaping the driving pulse one can control the spectral phase of the harmonics, as was shown in a recent study [54], allowing more control for compressing the attosecond pulses.

As an example, we numerically solve the time-dependent Schrödinger equation (TDSE) for a helium atom in a strong laser field to illustrate a possible use of our source for driving direct isolated soft-x-ray pulse generation (figure 16). The peak intensity of 6 × $10^{14}$ W cm$^{-2}$, which can be reached with a beam diameter of 27 $\mu$m, is chosen such that the total ionization is below the critical ionization level in helium [55]. The transmission and dispersion of the Sn filter are taken from [56]. Details about the TDSE solver are described in [33]. To gain more insight into the results given by the 3D TDSE simulation, we also calculated the ionization dynamics using the ADK formula (the blue curve in figure 16(a)) and the classical electron trajectories (overlaid on top of the spectrogram in figure 16(b)). Electron trajectories from three ionization events, which are labelled by numbers, are calculated and those trajectories that return to the ionized atom are shown in figure 16(b). For visualization, electrons ionized by the electric field with strength weaker than half of the maximum are neglected since they have negligible contribution to the HHG emission, as confirmed by the TDSE simulation.

With choice of CEPs as shown in figure 16(a), substantial ionization is limited to one optical half-cycle and an isolated soft-x-ray pulse spanning over 250 eV is generated (figures 16(b) and (c)) without the need for gating techniques or spectral filtering which typically limit the efficiency and the obtainable bandwidth. Using an additional Sn filter, which blocks the strong IR driving field and the nonlinearly chirped low-photon-energy spectral content below 70 eV, leads to an isolated 150 as pulse centred at 200 eV. Of note, the non-sinusoidal electric-field waveform leads to drastically changed electron trajectories (compared to those from a sinusoidal driving field) resulting in corresponding changes in quantum diffusion and atto-chirp, which can be controlled by means of the waveform synthesis parameters ($\phi_1$, $\phi_2$ and $\Delta t$).

In HHG, quantum diffusion and ionization rate are two competing factors in determining the ratio between radiation from long and short electron trajectories. While quantum diffusion always favours the short trajectories, when the HHG process is driven by conventional sinusoidal electric-field waveforms, the stronger ionization rate for the long trajectories results in significant radiation from electrons of both trajectories. For the example shown

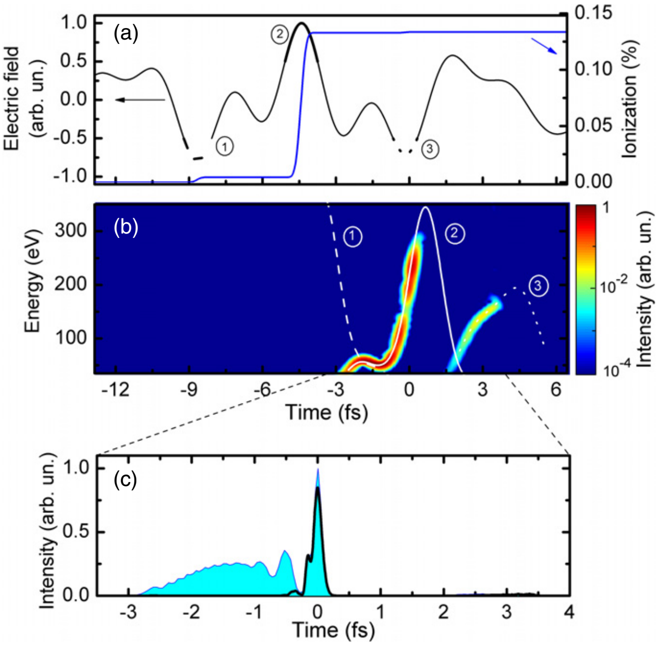

**Figure 16.** TDSE simulation results of the single-atom HHG with the synthesized waveforms. (a) Ionization dynamics (blue) induced in helium by a linearly polarized electric-field waveform (black) assuming a peak intensity of 6 × $10^{14}$ W cm$^{-2}$, $\phi_1 = 960$ mrad and $\phi_2 = -440$ mrad. (b) Spectrogram of the HHG superimposed with the calculated classical trajectories. Returning trajectories from three ionization events (2: the main pulse; 1 and 3: the satellite pulses) are shown for clear interpretation of the spectrogram. The synthesized pulse isolates the ionization process to a half optical cycle and a continuum spectrum spanning more than 250 eV can be achieved. The isolated soft-x-ray pulse has the same sign of chirp over 80% of the spectrum and so the compression setup can be simplified. (c) The isolated soft-x-ray pulse plotted in the time domain before (blue) and after (black line) a 100 nm thick Sn filter. The Sn filter is chosen for its capability to block the strong IR driving field and the nonlinearly chirped low-photon energy spectral content, and its good transmission in the soft-x-ray range. The filtered isolated soft-x-ray pulse has a FWHM duration of 150 as.

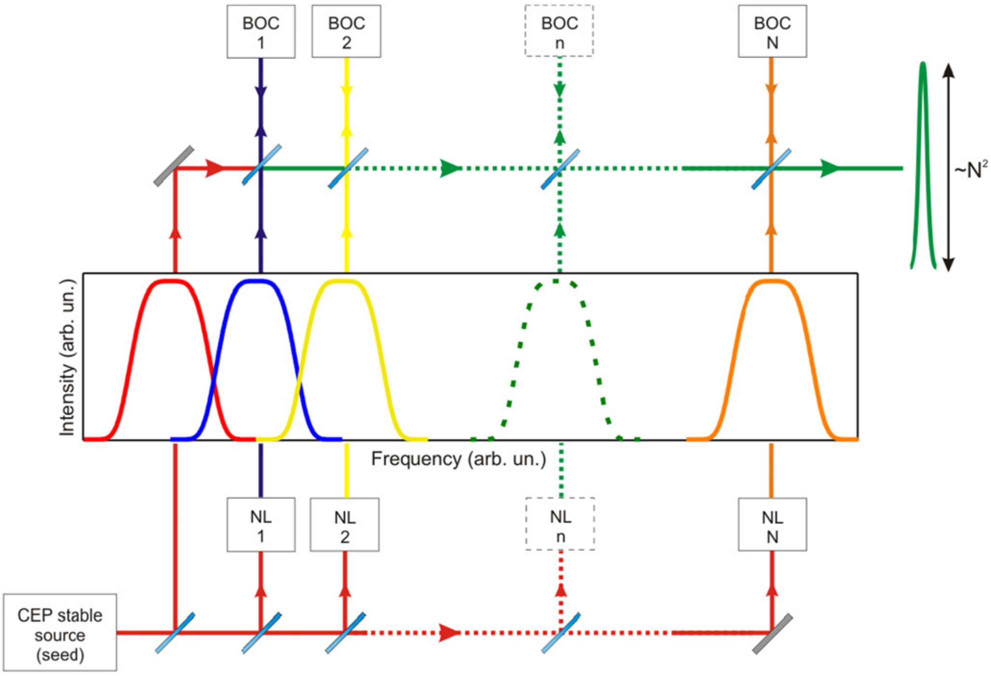

**Figure 17.** Scheme of the future scaled-up system. The demonstrated system is the prototype of a class of novel optical tools for attosecond control of strong-field physics experiments and it can be further scaled up in both optical bandwidth and pulse energy to fulfil the requirements of more demanding applications. BOC: balanced optical cross-correlator; NL: nonlinear effect.

in figure 16(b), where a sub-cycle waveform is used, the difference in travel time between long and short trajectories is increased. In addition, the ionization contribution to short trajectory radiation is boosted. Overall, quantum diffusion dominates over the ionization rate and effectively eliminates the radiation from long trajectories, resulting in isolated soft-x-ray pulse generation solely from short trajectories. This gives an example of the capability of our light source to simultaneously isolate the ionization process and manipulate electron trajectories within an optical cycle, allowing unprecedented control of the HHG process.

## 7. Conclusion

The concept and technology demonstrated here can be further scaled in both energy and bandwidth to expand its applicability to strong-field physics experiments. Pumped with a picosecond cryogenically cooled Yb:YAG laser, the pulse energy of the SWIR-OPCPA was recently scaled up to 850 $\mu$J [57]. In addition, since the feedback loop used for relative timing stabilization requires only a 30 Hz bandwidth, the system can be further scaled up to higher pulse energy at even lower repetition rate.

To avoid damage in the high-energy, picosecond Yb:YAG CPA system [58], a stretcher with a chirp rate of 1 ns nm$^{-1}$, which is twice as high as that of the current CFBG, is required. Besides, it has to be free of group-delay ripple (GDR) to ensure high quality of the stretched and re-compressed pulses [59]. Based on numerical modelling, we find that both amplitude and phase responses of the CFBG need to be carefully designed to prevent pulse distortions. Specifically, the GDR of the CFBG needs to be below 20 ps peak–peak deviation and the reflection amplitude shape must be closely approximated by a Gaussian profile. We note that CFBGs with low GDR have been extensively developed for applications in optical communication systems [60] and thus we are confident that superior performance can be achieved.

Figure 17 shows a schematic of a proposed scaled-up system. It comprises a number of OPCPAs seeded by a single CEP-stabilized light source both directly and through nonlinear effects which preserve the CEP stability such as intrapulse DFG, self-phase modulation and Raman shifting. The OPCPA pulses are combined in custom-made DM and the BOC-assisted feedback loops stabilize the relative timing. Different from the simple coherent beam combination of identical optical amplifiers, which leads to a linear peak-power scaling with the number of sub-modules, the proposed system increases the peak-power quadratically since both energy and bandwidth scale linearly with the number of sub-modules.

In conclusion, we have presented a scalable waveform synthesis scheme based on fully controlled coherent wavelength multiplexing of high-energy, few-cycle optical pulses from multi-colour OPCPAs. Currently, the system generates a non-sinusoidal waveform that can be used to drive physics experiments with an isolation of the strong-field phenomenon to a single optical cycle. The pulse energy is 15 $\mu$J with the spectrum spanning close to two octaves, and a numerical study shows the uniqueness of our source for direct isolated soft-x-ray pulse generation based on HHG, eliminating the need for gating techniques or spectral filtering. In addition to this application, this new high-intensity laser architecture can be applied to optical field-emission [61], tunnelling ionization studies [62], time-resolved spectroscopy

[63] and, in general, attosecond control of strong-field physics experiments.

## Acknowledgments

This work was supported by Air Force Office of Scientific Research grants FA9550-09-1-0212, FA8655-09-1-3101, FA9550-10-1-0063, the Center for Free-Electron Laser Science, the Australian Research Council Centre of Excellence for Ultrahigh bandwidth Devices for Optical Systems (project number CE110001018), and Progetto Roberto Rocca.

## References

[1] Jones D J *et al* 2000 Carrier-envelope phase control of femtosecond mode-locked lasers and direct optical frequency synthesis *Science* **288** 635
[2] Holzwarth R, Udem T, Hänsch T W, Knight J C, Wadsworth W J and Russell P S J 2000 Optical frequency synthesizer for precision spectroscopy *Phys. Rev. Lett.* **85** 2264
[3] Huang D *et al* 1991 Optical coherence tomography *Science* **254** 1178
[4] Li C-H *et al* 2008 A laser frequency comb that enables radial velocity measurements with a precision of 1 cm $s^{-1}$ *Nature* **452** 610
[5] Shank C V 1986 Investigation of ultrafast phenomena in the femtosecond time domain *Science* **233** 1276
[6] Zewail A H 1988 Laser femtochemistry *Science* **242** 1645
[7] Sundström V 2008 Femtobiology *Annu. Rev. Phys. Chem.* **59** 53
[8] Esarey E, Schroeder C B and Leemans W P 2009 Physics of laser-driven plasma-based electron accelerators *Rev. Mod. Phys.* **81** 1229
[9] Strickland D and Mourou G 1985 Compression of amplified chirped optical pulses *Opt. Commun.* **56** 219
[10] Corkum P B 1993 Plasma perspective on strong field multiphoton ionization *Phys. Rev. Lett.* **71** 1994
[11] Keldysh L V 1965 Ionization in the field of a strong electromagnetic wave *Sov. Phys.—JETP* **20** 1307
[12] Goulielmakis E *et al* 2008 Single-cycle nonlinear optics *Science* **320** 1614
[13] Krausz F and Ivanov M 2009 Attosecond physics *Rev. Mod. Phys.* **81** 163
[14] Schultze M *et al* 2010 Delay in photoemission *Science* **328** 1658
[15] Chipperfield L E, Robinson J S, Tisch J W G and Marangos J P 2009 Ideal waveform to generate the maximum possible electron recollision energy for any given oscillation period *Phys. Rev. Lett.* **102** 063003
[16] Matos L *et al* 2004 Direct frequency comb generation from an octave-spanning, prismless Ti:sapphire laser *Opt. Lett.* **29** 1683
[17] Gaydardzhiev A, Nikolov I, Buchvarov I, Petrov V and Noack F 2008 Ultrabroadband operation of a femtosecond optical parametric generator based on $BiB_3O_6$ in the near-IR *Opt. Express* **16** 2363
[18] Nisoli M, De Silvestri S and Svelto O 1996 Generation of high energy 10 fs pulses by a new pulse compression technique *Appl. Phys. Lett.* **68** 2793
[19] Chen X *et al* 2009 Generation of 4.3 fs, 1 mJ laser pulses via compression of circularly polarized pulses in a gas-filled hollow-core fiber *Opt. Lett.* **34** 1588
[20] Park J, Lee J-H and Nam C H 2009 Generation of 1.5 cycle 0.3 TW laser pulses using a hollow-fiber pulse compressor *Opt. Lett.* **34** 2342
[21] Bohman S, Suda A, Kanai T, Yamaguchi S and Midorikawa K 2010 Generation of 5.0 fs, 5.0 mJ pulses at 1 kHz using hollow-fiber pulse compression *Opt. Lett.* **35** 1887
[22] Harris S E and Sokolov A V 1998 Subfemtosecond pulse generation by molecular modulation *Phys. Rev. Lett.* **81** 2894
[23] Shverdin M Y, Walker D R, Yavuz D D, Yin G Y and Harris S E 2005 Generation of a single-cycle optical pulse *Phys. Rev. Lett.* **94** 033904
[24] Huang S W, Chen W-J and Kung A H 2006 Vibrational molecular modulation in hydrogen *Phys. Rev.* A **74** 063825
[25] Chen W-J *et al* 2008 Sub-single-cycle optical pulse train with constant carrier envelope phase *Phys. Rev. Lett.* **100** 163906
[26] Chan H-S *et al* 2011 Synthesis and measurement of ultrafast waveforms from five discrete optical harmonics *Science* **331** 1165
[27] Wirth A *et al* 2011 Synthesized light transients *Science* **334** 6053
[28] Wei Z, Kobayashi Y, Zhang Z and Torizuka K 2001 Generation of two-color femtosecond pulses by self-synchronizing Ti:sapphire and Cr:forsterite lasers *Opt. Lett.* **26** 1806
[29] Shelton R K, Ma L-S, Kapteyn H C, Murnane M M, Hall J L and Ye J 2001 Phase-coherent optical pulse synthesis from separate femtosecond lasers *Science* **293** 1286
[30] Krauss G *et al* 2010 Synthesis of a single cycle of light with compact erbium-doped fibre technology *Nat. Photon.* **4** 33
[31] Dubietis A, Butkus R and Piskarskas A P 2006 Trends in chirped pulse optical parametric amplification *IEEE J. Sel. Top. Quantum Electron.* **12** 163
[32] Haessler S, Balčiūnas T, Salières P and Baltuška A 2011 Challenges in self-probing of molecules, to be met by a waveform synthesizer *3rd Int. Conf. on Attosecond Physics (Sapporo, Japan)* E-2
[33] Huang S-W *et al* 2011 High-energy pulse synthesis with sub-cycle waveform control for strong-field physics *Nature Photonics* **5** 475
[34] Schibli T R *et al* 2003 Attosecond active synchronization of passively mode-locked lasers by balanced cross correlation *Opt. Lett.* **28** 947
[35] Ross I N, Matousek P, New G H C and Osvay K 2002 Analysis and optimization of optical parametric chirped pulse amplification *J. Opt. Soc. Am.* B **19** 2945
[36] Miura T, Kobayashi K, Takasago K, Zhang Z, Torizuka K and Kannari F 2000 Timing jitter in a kilohertz regenerative amplifier of a femtosecond-pulse Ti:$Al_2O_3$ laser *Opt. Lett.* **25** 1795
[37] Moses J, Manzoni C, Huang S-W, Cerullo G and Kärtner F X 2009 Temporal optimization of ultrabroadband high-energy OPCPA *Opt. Express* **17** 5540
[38] Manzoni C, Moses J, Kärtner F X and Cerullo G 2011 Excess quantum noise in optical parametric chirped-pulse amplification *Opt. Express* **19** 8357
[39] Moses J *et al* 2009 Highly stable ultrabroadband mid-IR optical parametric chirped-pulse amplifier optimized for superfluorescence suppression *Opt. Lett.* **34** 1639
[40] Chang Z 2006 Carrier-envelope phase shift caused by grating-based stretchers and compressors *Appl. Opt.* **45** 8350
[41] Baltuška A, Fuji T and Kobayashi T 2002 Controlling the carrier-envelope phase of ultrashort light pulses with optical parametric amplifiers *Phys. Rev. Lett.* **88** 133901
[42] Zou Q and Lü B 2007 Propagation properties of ultrashort pulsed beams with constant waist width in free space *Opt. Laser Technol.* **39** 619
[43] Birge J R, Crespo H M and Kärtner F X 2010 Theory and design of two-dimensional spectral shearing interferometry for few-cycle pulse measurement *J. Opt. Soc. Am.* B **27** 1165
[44] Iaconis C and Walmsley I A 1999 Self-referencing spectral interferometry for measuring ultrashort optical pulses *IEEE J. Quantum Electron.* **35** 501

[45] Wittmann T *et al* 2009 Single-shot carrier-envelope phase measurement of few-cycle laser pulses *Nature Phys.* **5** 357

[46] Mücke O D *et al* 2009 Scalable Yb-MOPA-driven carrier-envelope phase-stable few-cycle parametric amplifier at 1.5 $\mu$m *Opt. Lett.* **34** 118

[47] Chang Z, Shan B and Ghimire S 2005 Generation of the attosecond extreme ultraviolet supercontinuum by a polarization gating *J. Mod. Opt.* **52** 277

[48] Sansone G *et al* 2006 Isolated single-cycle attosecond pulses *Science* **314** 443

[49] Kim I J *et al* 2005 Highly efficient high-harmonic generation in an orthogonally polarized two-color laser field *Phys. Rev. Lett.* **94** 243901

[50] Oishi Y, Kaku M, Suda A, Kannari F and Midorikawa K 2006 Generation of extreme ultraviolet continuum radiation driven by a sub-10-fs two-color field *Opt. Express* **14** 7230

[51] Abel M J *et al* 2009 Isolated attosecond pulses from ionization gating of high-harmonic emission *Chem. Phys.* **366** 9

[52] Mashiko H *et al* 2008 Double optical gating of high-order harmonic generation with carrier-envelope phase stabilized lasers *Phys. Rev. Lett.* **100** 103906

[53] Ferrari F *et al* 2010 High-energy isolated attosecond pulses generated by above-saturation few-cycle fields *Nature Photonics* **4** 875

[54] Dudovich N *et al* 2006 Measuring and controlling the birth of attosecond XUV pulses *Nature Phys.* **2** 781

[55] Popmintchev T *et al* 2009 Phase matching of high harmonic generation in the soft and hard x-ray regions of the spectrum *Proc. Natl Acad. Sci. USA* **106** 10516

[56] Henke B 1993 X-ray interactions: photoabsorption, scattering, transmission, and reflection at E = 50–30000 eV, Z = 1–92 *At. Data Nucl. Data Tables* **54** 181

[57] Hong K-H *et al* 2011 High-energy, phase-stable, ultrabroadband kHz OPCPA at 2.1$\mu$m pumped by a picosecond cryogenic Yb:YAG laser *Opt. Express* **19** 15538

[58] Hong K-H *et al* 2010 High-energy, kHz-repetition-rate, ps cryogenic Yb:YAG chirped-pulse amplifier *Opt. Lett.* **35** 1752

[59] Littler I C M, Fu L and Eggleton B J 2005 Effect of group delay ripple on picosecond pulse compression schemes *Appl. Opt.* **44** 4702

[60] Eggleton B J, Rogers J A, Westbrook P S and Strasser T A 1999 Electrically tunable power efficient dispersion compensating fiber Bragg grating *IEEE Photonics Technol. Lett.* **11** 854

[61] Hommelhoff P, Kealhofer C and Kasevich M A 2006 Ultrafast electron pulses from a tungsten tip triggered by low-power femtosecond laser pulses *Phys. Rev. Lett.* **97** 247402

[62] Arissian L *et al* 2010 Direct test of laser tunneling with electron momentum imaging *Phys. Rev. Lett.* **105** 133002

[63] Hochstrasser R M 2007 Two-dimensional spectroscopy at infrared and optical frequencies *Proc. Natl Acad. Sci. USA* **104** 14190